Letters

Optimized Branch Current Control of Modular Multilevel Matrix Converters Under Branch Fault Conditions

Boran Fan, Kui Wang, Zedong Zheng, Lie Xu, and Yongdong Li

***Abstract*—The modular multilevel matrix converter (M3C) is a promising topology for high-voltage high-power applications. It features easy scalability, high-quality input and output waveforms, superior availability, etc. This letter aims to further increase the availability of the M3C when one or more of the nine branches are lost. A general nonlinear multivariable optimization model is set up to optimize the branch current configuration after the branch lost. The proposed method reduces system power capability loss after the branch failure. It achieves a smooth transition from a full M3C to a reduced topology without shutdown of the system. A M3C prototype with 27 cells is designed, and experiment results are presented to confirm the validity of this method.**

***Index Terms*—Branch failure, fault tolerance, Hexverter, modular multilevel matrix converter (M3C), triple star-bridge cells (TSBC) converter.**

I. Introduction

MODULAR multilevel topologies, such as the modular multilevel converter (MMC) and the modular multilevel matrix converter (M3C), have many advantages in high-voltage high-power applications [1]. The MMC has been successfully used in high-voltage direct-current (HVDC) transmissions. Compared with the MMC, the M3C has improved capacitor-voltage fluctuation characteristics at low-frequency operation [2]–[4]. This advantage makes the M3C more suitable for adjustable speed drive applications. In addition, similar with HVDC transmission of the MMC, the M3C has a "counterpart application" in the fractional frequency transmission system [5], a promising solution for offshore wind power transmission. For these applications, reliability is of great importance, and fortunately, due to the modular structure, converters such as the MMC and the M3C have superior availability. Several failed modules do not necessarily cause system shutdown. To fully take the advantage, many works have been conducted to develop appropriate operation strategies with failed modules in both the MMC [6] and the M3C [7].

Compared with the module fault, complete branch loss is a more serious failure, and few papers have discussed much about it. Such a failure can be caused by too many failed modules in one branch: a mechanical connection failure, control unit error, etc. To increase system availability under branch fault conditions, Karwatzki *et al*. [8] proposed an inspiring fault-tolerance strategy for the M3C. After the branch failure, the nine-branch M3C was reduced and operated as a six-branch Hexverter [9]. It allows a further increase of the M3C high availability. However, there are two drawbacks of the strategy: the first is that the converter suffers a considerable power capability loss because when a single branch is lost, two additional nonfailure branches need to be symmetrically removed; the second is that as the converter is operated as a Hexverter, large common-mode voltage (CMV) and circulating current injections are required when reactive power difference exists between the input and output three-phase systems [10].

This letter aims to propose a strategy to use all the remaining branches of the M3C after the branch failure. It helps to optimize the converter performance after a branch lost. The biggest challenge lies in the appropriate current configuration for the remaining branches. Section II equalizes the branch current configuration to the solving of a nonlinear multivariable optimization problem. Taking the eight-branch topology as an example, Section III solves the optimization problem established in Section II and presents the optimized branch current configuration. Experimental results in Section IV validate a smooth transition from a full M3C to the eight-branch topology and a stable operation of the reduced topology after the branch failure. Section V concludes this letter.

II. Optimization-Based Branch Current Configuration Strategy

Fig. 1 shows the circuit configuration of the M3C. It connects two three-phase systems with nine branches. Each branch consists of a branch inductor L_b and a string of cascaded full-bridge cells. The input and output three-phase systems are denoted as "*UVW*" and "*RST*." S_i ($i = 1, 2, \ldots, 9$) are branch breakers. If "$S_i = 1$," the breaker is closed and the branch is connected;

Manuscript received September 5, 2017; revised September 28, 2017; accepted October 19, 2017. Date of publication November 2, 2017; date of current version February 22, 2018. This work was supported by the Education Development Program of Delta Environmental and Educational Foundation under Grant DREK2015001. *(Corresponding author: Zedong Zheng.)*

The authors are with the State Key Laboratory of Power System, Department of Electrical Engineering, Tsinghua University, Beijing 100084, China (e-mail: fbr13@mails.tsinghua.edu.cn; wangkui@tsinghua.edu.cn; zzd@tsinghua.edu.cn; xulie@tsinghua.edu.cn; liyd@tsinghua.edu.cn).

Color versions of one or more of the figures in this letter are available online at http://ieeexplore.ieee.org.

Digital Object Identifier 10.1109/TPEL.2017.2769117

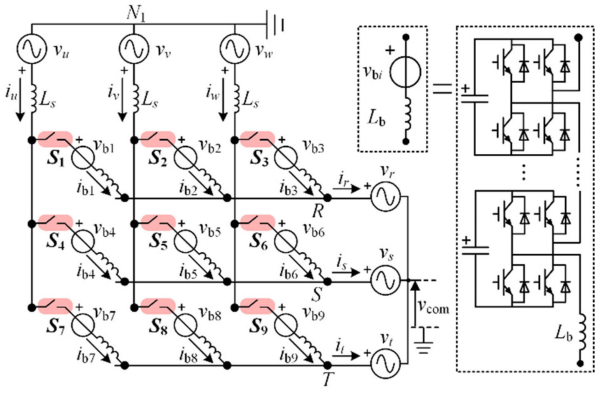

Fig. 1. Circuit configuration of the M3C. S_i $(i = 1, 2, \ldots, 9)$ are branch breakers.

otherwise, if "$S_i = 0$," the breaker is opened and the branch is removed.

In the following analysis, the input and output systems are assumed three-phase balanced. The input side is connected with an ac grid. Voltages and currents in the $\alpha\beta$ reference frame are defined as in (1). The definition ensures unity power factor at the ac grid

$$\begin{aligned} u_\alpha^{uvw} &= \hat{v}_{m1}\cos(\omega_1 t), \quad u_\beta^{uvw} = \hat{v}_{m1}\sin(\omega_1 t) \\ i_\alpha^{uvw} &= \hat{i}_{m1}\cos(\omega_1 t), \quad i_\beta^{uvw} = \hat{i}_{m1}\sin(\omega_1 t) \\ u_\alpha^{rst} &= \hat{v}_{m2}\cos(\omega_2 t + \theta), \quad u_\beta^{rst} = \hat{v}_{m2}\sin(\omega_2 t + \theta) \\ i_\alpha^{rst} &= \hat{i}_{m2}\cos(\omega_2 t + \theta - \varphi_2), \quad i_\beta^{rst} = \hat{i}_{m2}\sin(\omega_2 t + \theta - \varphi_2). \end{aligned} \tag{1}$$

Nine branch currents are defined in (2), which contain frequency components of the input and output systems. In (2), k_{ij} $(i = 1, 2, \ldots, 9,\ j = 1, 2, 3, 4)$ are the 36 variables that determine the branch current configuration

$$\begin{aligned} i_{bi} &= k_{i1}\cdot i_\alpha^{uvw} + k_{i2}\cdot i_\beta^{uvw} + k_{i3}\cdot i_\alpha^{rst} + k_{i4}\cdot i_\beta^{rst}, \\ & i = 1, 2, ..., 9. \end{aligned} \tag{2}$$

In the M3C, the nine branch currents synthesize the input and output three-phase currents. This requires the 36 variables in (2) satisfy the equality constraints in (3) shown at the bottom of this page. In this letter, constraints in (3) are denoted as the "First set of equality constraints."

Meanwhile, the branch current configuration, defined in (2), should ensure dc power on each branch to be zero; otherwise, the floating capacitor-voltage will become unstable. Since the CMV injection may cause problems like overmodulation, motor insulation damage and etc. In this letter, the injection of the CMV is avoided. As a result, taking the first branch as an example, the dc component of the branch power can be calculated as follows. Here, the input and output system frequencies are assumed different

$$\left.\begin{aligned} u_{b1} &= u_u - u_r = u_\alpha^{uvw} - u_\alpha^{rst} \\ i_{b1} &= k_{11}\cdot i_\alpha^{uvw} + k_{12}\cdot i_\beta^{uvw} + k_{13}\cdot i_\alpha^{rst} + k_{14}\cdot i_\beta^{rst} \end{aligned}\right\} \Rightarrow$$
$$\begin{aligned} p_{b1}^{\mathrm{dc}} &= \overline{u_{b1}\cdot i_{b1}} = (k_{11}\cos\varphi_2 - k_{13}\cos\varphi_2 + k_{14}\sin\varphi_2) \\ &\quad \cdot \hat{v}_{m2}\hat{i}_{m2}. \end{aligned} \tag{4}$$

By calculating dc power of the nine branches and assigning them to be zero, the 36 variables in (2) should satisfy the equality constraints in (5) shown at the bottom of this page. In this letter, constraints in (5) are denoted as the "Second set of equality constraints."

In Fig. 1, the status of S_i decides whether a branch is connected or removed. Obviously, no matter the status of S_i, equality constraints in (3) and (5) are prerequisites for the stable

$$\begin{cases} i_{b1}+i_{b2}+i_{b3} = i_u = i_\alpha^{uvw} \\ i_{b4}+i_{b5}+i_{b6} = i_v = (-i_\alpha^{uvw} + \sqrt{3}i_\beta^{uvw})/2 \\ i_{b7}+i_{b8}+i_{b9} = i_w = (-i_\alpha^{uvw} - \sqrt{3}i_\beta^{uvw})/2 \\ i_{b1}+i_{b4}+i_{b7} = i_r = i_\alpha^{rst} \\ i_{b2}+i_{b5}+i_{b8} = i_s = (-i_\alpha^{rst} + \sqrt{3}i_\beta^{rst})/2 \\ i_{b3}+i_{b6}+i_{b9} = i_t = (-i_\alpha^{rst} - \sqrt{3}i_\beta^{rst})/2 \end{cases} \Rightarrow \begin{cases} k_{11}+k_{21}+k_{31} = 1 \\ k_{1i}+k_{2i}+k_{3i} = 0,\ i = 2,3,4 \\ k_{41}+k_{51}+k_{61} = -1/2 \\ k_{42}+k_{52}+k_{62} = \sqrt{3}/2 \\ k_{4i}+k_{5i}+k_{6i} = 0,\ i = 3,4 \\ k_{71}+k_{81}+k_{91} = -1/2 \\ k_{72}+k_{82}+k_{92} = -\sqrt{3}/2 \\ k_{7i}+k_{8i}+k_{9i} = 0,\ i = 3,4 \end{cases}, \quad \begin{cases} k_{1i}+k_{4i}+k_{7i} = 0,\ i = 1,2,4 \\ k_{13}+k_{43}+k_{73} = 1 \\ k_{2i}+k_{5i}+k_{8i} = 0,\ i = 1,2 \\ k_{23}+k_{53}+k_{83} = -1/2 \\ k_{24}+k_{54}+k_{84} = \sqrt{3}/2 \\ k_{3i}+k_{6i}+k_{9i} = 0,\ i = 1,2 \\ k_{33}+k_{63}+k_{93} = -1/2 \\ k_{34}+k_{64}+k_{94} = -\sqrt{3}/2 \end{cases} \tag{3}$$

$$p_{bi}^{\mathrm{dc}} = 0,\ i = 1, 2, ..9 \Rightarrow \begin{cases} \cos\varphi_2\cdot k_{11} - \cos\varphi_2\cdot k_{13} + k_{14}\cdot\sin\varphi_2 = 0 \\ 2\cos\varphi_2\cdot k_{21} + (\cos\varphi_2 - \sqrt{3}\sin\varphi_2)\cdot k_{23} - (\sin\varphi_2 + \sqrt{3}\cos\varphi_2)\cdot k_{24} = 0 \\ 2\cos\varphi_2\cdot k_{31} + (\cos\varphi_2 + \sqrt{3}\sin\varphi_2)\cdot k_{33} - (\sin\varphi_2 - \sqrt{3}\cos\varphi_2)\cdot k_{34} = 0 \\ (-\cos\varphi_2)\cdot k_{41} + (\sqrt{3}\cos\varphi_2)\cdot k_{42} - 2\cos\varphi_2\cdot k_{43} + 2\sin\varphi_2\cdot k_{44} = 0 \\ (-\cos\varphi_2)\cdot k_{51} + (\sqrt{3}\cos\varphi_2)\cdot k_{52} + (\cos\varphi_2 - \sqrt{3}\sin\varphi_2)\cdot k_{53} - (\sin\varphi_2 + \sqrt{3}\cos\varphi_2)\cdot k_{54} = 0 \\ (-\cos\varphi_2)\cdot k_{61} + (\sqrt{3}\cos\varphi_2)\cdot k_{62} + (\cos\varphi_2 + \sqrt{3}\sin\varphi_2)\cdot k_{63} - (\sin\varphi_2 - \sqrt{3}\cos\varphi_2)\cdot k_{64} = 0 \\ (-\cos\varphi_2)\cdot k_{71} - (\sqrt{3}\cos\varphi_2)\cdot k_{72} - 2\cos\varphi_2\cdot k_{73} + 2\sin\varphi_2\cdot k_{74} = 0 \\ (-\cos\varphi_2)\cdot k_{81} - (\sqrt{3}\cos\varphi_2)\cdot k_{82} + (\cos\varphi_2 - \sqrt{3}\sin\varphi_2)\cdot k_{83} - (\sin\varphi_2 + \sqrt{3}\cos\varphi_2)\cdot k_{84} = 0 \\ (-\cos\varphi_2)\cdot k_{91} - (\sqrt{3}\cos\varphi_2)\cdot k_{92} + (\cos\varphi_2 + \sqrt{3}\sin\varphi_2)\cdot k_{93} - (\sin\varphi_2 - \sqrt{3}\cos\varphi_2)\cdot k_{94} = 0 \end{cases} \tag{5}$$

TABLE I
BRANCH CURRENT CONFIGURATION

Topology	M3C	Hexverter	8-Branch
Branch Breakers	$S_i = 1, i = 1, 2, ..9$	$S_i = 0$ when $i = 3, 5, 7$ else $S_i = 1$	$S_i = 0$ when $i = 3$ else $S_i = 1$
$\cos\varphi_2$	Any	± 1	± 1
$[k_{ij}] =$	$\begin{bmatrix} k_{11} & k_{12} & k_{13} & k_{14} \\ k_{21} & k_{22} & k_{23} & k_{24} \\ k_{31} & k_{32} & k_{33} & k_{34} \\ k_{41} & k_{42} & k_{43} & k_{44} \\ k_{51} & k_{52} & k_{53} & k_{54} \\ k_{61} & k_{62} & k_{63} & k_{64} \\ k_{71} & k_{72} & k_{73} & k_{74} \\ k_{81} & k_{82} & k_{83} & k_{84} \\ k_{91} & k_{92} & k_{93} & k_{94} \end{bmatrix}$	$\frac{1}{6}\begin{bmatrix} 2 & 0 & 2 & 0 \\ 2 & 0 & -1 & \sqrt{3} \\ 2 & 0 & -1 & -\sqrt{3} \\ -1 & \sqrt{3} & 2 & 0 \\ -1 & \sqrt{3} & -1 & \sqrt{3} \\ -1 & \sqrt{3} & -1 & -\sqrt{3} \\ -1 & -\sqrt{3} & 2 & 0 \\ -1 & -\sqrt{3} & -1 & -\sqrt{3} \\ -1 & -\sqrt{3} & -1 & -\sqrt{3} \end{bmatrix}$	$\frac{1}{6}\begin{bmatrix} 3 & -\sqrt{3} & 3 & -\sqrt{3} \\ 3 & \sqrt{3} & -3 & \sqrt{3} \\ 0 & 0 & 0 & 0 \\ -3 & \sqrt{3} & 3 & \sqrt{3} \\ 0 & 0 & 0 & 0 \\ 0 & 2\sqrt{3} & -3 & -\sqrt{3} \\ 0 & 0 & 0 & 0 \\ -3 & -\sqrt{3} & 0 & 2\sqrt{3} \\ 0 & -2\sqrt{3} & 0 & -2\sqrt{3} \end{bmatrix}$	$\frac{1}{12}\begin{bmatrix} 6 & 0 & 6 & -2\sqrt{3} \\ 6 & 0 & -6 & 2\sqrt{3} \\ 0 & 0 & 0 & 0 \\ -3 & \sqrt{3} & 3 & \sqrt{3} \\ -3 & \sqrt{3} & 0 & 2\sqrt{3} \\ 0 & 4\sqrt{3} & -3 & -3\sqrt{3} \\ -3 & -\sqrt{3} & 3 & \sqrt{3} \\ -3 & -\sqrt{3} & 0 & 2\sqrt{3} \\ 0 & -4\sqrt{3} & -3 & -3\sqrt{3} \end{bmatrix}$
Branch current configuration	$\begin{cases} i_{b1} = (i_u + i_r)/3 \\ i_{b2} = (i_u + i_s)/3 \\ i_{b3} = (i_u + i_t)/3 \\ i_{b4} = (i_v + i_r)/3 \\ i_{b5} = (i_v + i_s)/3 \\ i_{b6} = (i_v + i_t)/3 \\ i_{b7} = (i_w + i_r)/3 \\ i_{b8} = (i_w + i_s)/3 \\ i_{b9} = (i_w + i_t)/3 \end{cases}$	$\begin{cases} i_{b1} = (i_u - i_v + i_r - i_s)/3 \\ i_{b2} = (i_u - i_w + i_s - i_r)/3 \\ i_{b3} = 0 \\ i_{b4} = (i_v - i_u + i_r - i_t)/3 \\ i_{b5} = 0 \\ i_{b6} = (i_v - i_w + i_t - i_r)/3 \\ i_{b7} = 0 \\ i_{b8} = (i_w - i_u + i_s - i_t)/3 \\ i_{b9} = (i_w - i_v + i_t - i_s)/3 \end{cases}$	$\begin{cases} i_{b1} = (3i_u + 2i_r - 2i_s)/6 \\ i_{b2} = (3i_u - 2i_r + 2i_s)/6 \\ i_{b3} = 0 \\ i_{b4} = (-i_u + i_v + i_r - i_t)/6 \\ i_{b5} = (-i_u + i_v + i_s - i_t)/6 \\ i_{b6} = (2i_v - 2i_w + 3i_t)/6 \\ i_{b7} = (-i_u + i_w + i_r - i_t)/6 \\ i_{b8} = (-i_u + i_w + i_s - i_t)/6 \\ i_{b9} = (-2i_v + 2i_w + 3i_t)/6 \end{cases}$
Branch current Magnitude $\hat{i}_{bi}$	$\frac{\hat{i}_{m1}+\hat{i}_{m2}}{3}, i = 1, 2, ..9.$	$\begin{cases} \frac{\hat{i}_{m1}+\hat{i}_{m2}}{\sqrt{3}} & i = 1, 2, 4, 6, 8, 9 \\ 0 & i = 3, 5, 7. \end{cases}$	$\begin{cases} (\sqrt{3}\hat{i}_{m1} + 2\hat{i}_{m2}) \cdot \sqrt{3}/6 & i = 1, 2 \\ (2\hat{i}_{m1} + \sqrt{3}\hat{i}_{m2}) \cdot \sqrt{3}/6 & i = 6, 8, 9 \\ (\hat{i}_{m1} + \hat{i}_{m2}) \cdot \sqrt{3}/6 & i = 4, 5, 7 \\ 0 & i = 3. \end{cases}$

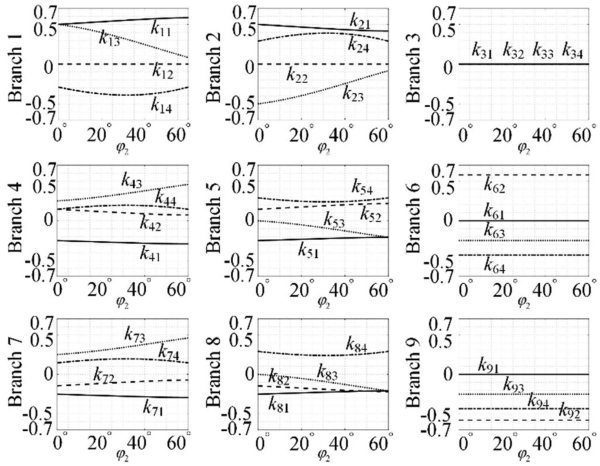

Fig. 2. Solution of the optimization problem when branch 3 is lost. The value of the optimized 36 variables ($k_{ij}, i = 1, 2, \ldots, 9, j = 1, 2, 3, 4$) changes with output power factor angle φ_2.

operation of the converter. For the branch fault condition, if a branch is lost or removed, since the relative branch current is zero, a set of additional constraints is necessary as shown in (6). The constraints in (6) are denoted as the "Third set of equality constraints"

$$\text{if } S_i = 0, i = 1, 2, ..9 \;\Rightarrow\; k_{i1} = 0, k_{i2} = 0, k_{i3} = 0, k_{i4} = 0. \tag{6}$$

Based on the three sets of equality constraints in (3), (5), and (6), taking k_{ij} as the variables, a nonlinear optimization problem is set up in (7). The objective function J in (7) helps to limit the branch current magnitude. It is worth mentioning that the definition of the objective function J is not exclusive. It can be adjusted based on application demands

$$\text{Minimize } J = \sum_{i=1}^{9}\sum_{j=1}^{4} k_{ij}^2$$
$$\text{such that } \begin{cases} \text{First set of equality constraints} & \text{[see (3)]} \\ \text{Second set of equality constraints} & \text{[see (5)]} \\ \text{Thirdset of equality constraints} & \text{[see (6)].} \end{cases} \tag{7}$$

In (7), the objective function J and the first set of equality constraints are independent of circuit parameters. According to (5) and (6), the second and third sets of equality constraints are affected by output power factor angle φ_2 and breaker status S_i, respectively. For a specified φ_2 and a set of S_i, by solving the problem in (7), an optimized branch current configuration can be achieved.

III. BRANCH CURRENT CONFIGURATION OF THE EIGHT-BRANCH TOPOLOGY

Section II proposes an optimization-based strategy to get the branch current configuration. This section will first verify the proposed strategy on the M3C and the Hexverter and, then, use the strategy to obtain the branch current configuration when a single branch is lost. Since (7) is a nonlinear optimization problem with linear constraints, it can be easily solved by using the "fmincon" solver in MATLAB, or more specifically, since it is a linearly constrained quadratic optimization problem, it can also be solved by the "quadprog" solver.

For the M3C, since all the branch breakers are closed, the third set of equality constraints in (6) does not exist. The solution of

TABLE II
EXPERIMENT PARAMETERS

M3C Parameters			Experiment Condition			Optimization solution $[k_{ij}]$
Parameters	Symbol	Value	Parameters	Symbol	Value	
Switching Frequency	f_s	2kHz	Grid frequency	f_1	50Hz	$\begin{bmatrix} 0.512 & 0 & 0.4709 & -0.327 \\ 0.488 & 0 & -0.4709 & 0.327 \\ 0 & 0 & 0 & 0 \\ -0.256 & 0.1339 & 0.2645 & 0.1635 \\ -0.244 & 0.1548 & -0.0145 & 0.2695 \\ 0 & 0.5774 & -0.25 & -0.433 \\ -0.256 & -0.1339 & 0.2645 & 0.1635 \\ -0.244 & -0.1548 & -0.0145 & 0.2695 \\ 0 & -0.5774 & -0.25 & -0.433 \end{bmatrix}$
Cells per branch	N	3	Grid Voltage Magnitude	$\hat{v}_{m1}$	160V	
Module Capacitance	C	880uF	Output frequency	f_2	30Hz	
Branch inductance	L_b	2mH	Output Voltage Magnitude	$\hat{v}_{m2}$	200V	
AC grid inductance	L_s	5mH	Load Resistance	R	15Ω	
Capacitor Voltage	U_c*	155V	Load Inductance	L	10mH	

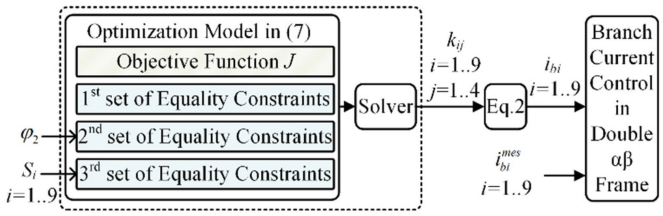

Fig. 3. Overall control strategy.

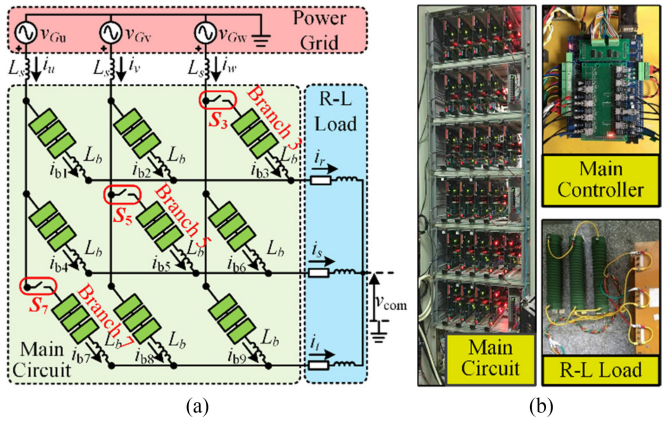

Fig. 4. (a) Circuit configuration. (b) Photos of the M3C experiment platform.

the optimization problem $[k_{ij}]$ is shown in the fourth line, second column in Table I. According to (2) and by applying an inverse park transformation, the branch current configuration can be written by system input and output currents as shown in the fifth line, second column in Table I. The branch current coincides with previous research [11]–[13]. For the M3C, the solution of (7) remains the same as power factor angle φ_2 changes, which indicates that the optimized branch current configuration of the M3C is independent of φ_2.

For the Hexverter, assume that branches 3, 5, and 7 in Fig. 1 are removed ($S_i = 0, i = 3, 5, 7$). The solution of the optimization problem $[k_{ij}]$ is shown in the fourth line, third column in Table I and the branch current configuration in the fifth line, same column. It can be seen that the branch current coincides with previous research [14]. Besides, the optimization has a solution only when φ_2 satisfies "$\cos\varphi_2 = \pm 1$." This is because, as explained in Section II, the proposed strategy ensures unity power factor at input side and no CMV injected. In this case, if "$\cos\varphi_2 \neq \pm 1$," reactive power difference exists between the input and output systems. Without branch power compensation provided by the CMV, the branch dc power is not zero and capacitor-voltage in the Hexverter is unstable [15], which makes the second set of equality constraints in (5) not hold; therefore, no solution can be found when $\cos\varphi_2 \neq \pm 1$ for the Hexverter.

For the branch fault condition of the M3C, without loss of generality, assume that branch 3 is lost ($S_3 = 0$). By solving the problem in (7), the branch current configuration on the eight remaining branches can be achieved. In the condition of "$\cos\varphi_2 = \pm 1$," the solution of the optimization problem $[k_{ij}]$ is shown in the fourth line, fourth column in Table I and the branch current configuration in the fifth line, same column. The branch current configuration characteristic of the eight-branch topology lies between the M3C and the Hexverter. Unlike the Hexverter, when φ_2 does not satisfy "$\cos\varphi_2 = \pm 1$," the eight-branch topology still have solutions for the optimization problem in (7). It indicates when input and output three-phase systems have reactive power difference, CMV injection is not indispensable for the eight-branch topology, which is similar as the M3C. This is a significant advantage for real application. Meanwhile, different from the M3C, the optimized branch current configuration of the eight-branch topology differentiates with the change of φ_2. The solution $[k_{ij}]$ under different φ_2 is shown in Fig. 2. As explained at the end of Section II, for a specified topology, the solution $[k_{ij}]$ is only affected by φ_2. So, in real application, Fig. 2 can be stored as a lookup table and the optimized branch current configuration can be selected according to the value of φ_2.

The last line of Table I shows the branch current magnitude comparison of the M3C, the Hexverter, and the eight-branch topology. Assuming that input and output systems share a same current magnitude ($\hat{i}_{m1} = \hat{i}_{m2}$), the maximum branch current magnitude of the eight-branch topology is 7.2% lower than the Hexverter. It suggests a larger power capability after the branch lost if the M3C is operated as an eight-branch topology instead of a Hexverter. Moreover, if there is reactive power at the load side, the Hexverter will require considerable CMV and circulating current injection, which gives the eight-branch topology an even larger power margin. Besides, according to the last line of Table I, branch currents on the eight-branch topology is smaller than the Hexverter, and therefore, the eight-branch topology can have a reduced capacitor-voltage fluctuation compared to the Hexverter.

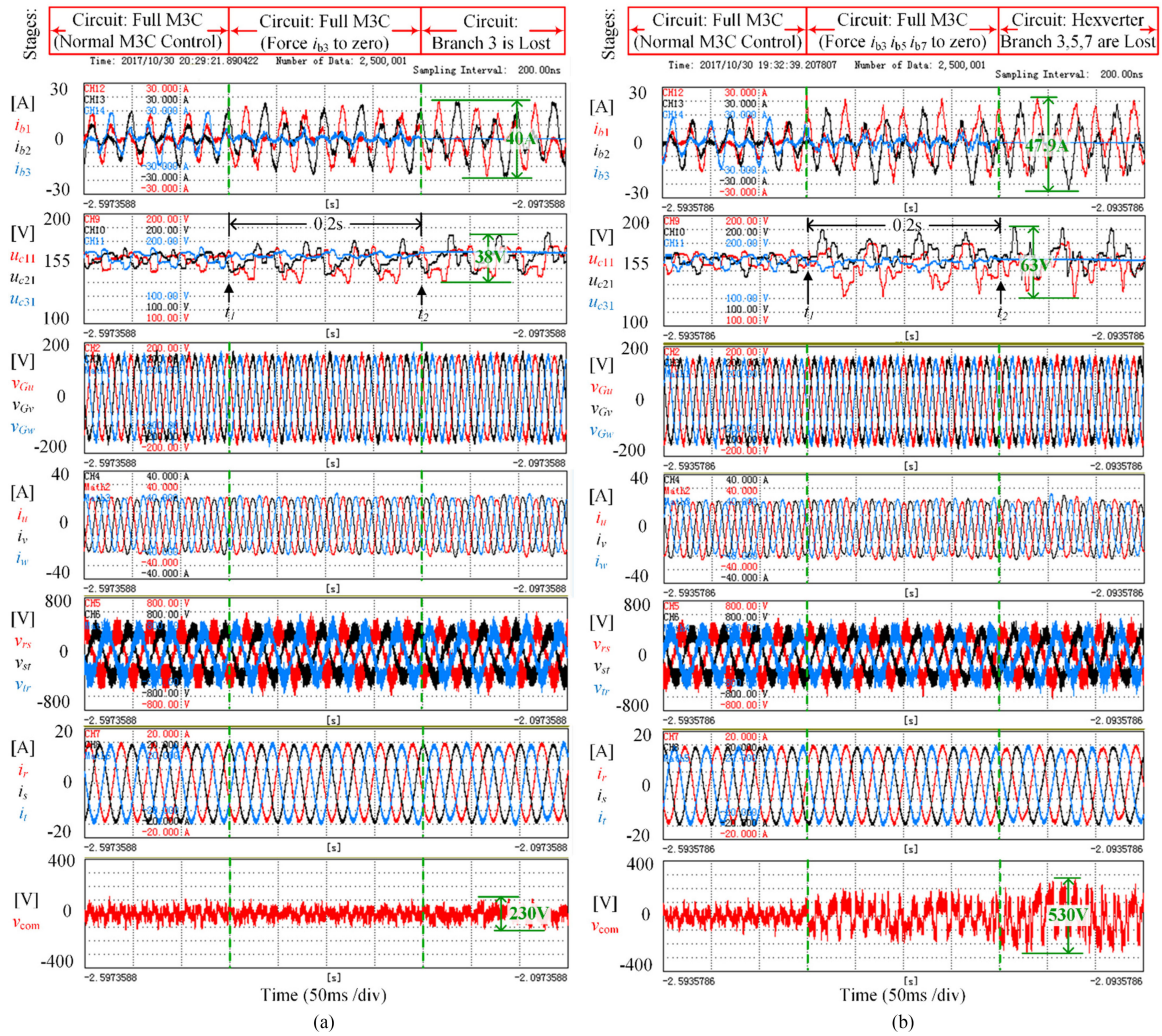

Fig. 5. (a) Verification of the transition from full M3C to the eight-branch topology. (b) Transition from full M3C to the Hexverter topology. (From top to bottom: Branch currents, capacitor voltages, ac grid phase-to-neutral voltages, input three-phase currents, output line-to-line voltages, output three-phase currents, and CMV v_{com}.)

In this section, a detailed branch current configuration is provided for the eight-branch topology. Taking these branch currents as the reference value, in practice, actual branch currents can then be controlled to follow these references by using the well-established current control method established in the double-$\alpha\beta$ frame [11]–[13]. The overall control strategy is shown in Fig. 3, where i_{bi} refers to the optimized branch current configuration and i_{bi}^{mes} refers to the measured branch currents. The optimization process shown in the dashed box is performed offline, and the optimization results (k_{ij}) are stored as lookup tables in a real-time system.

IV. Experiment Results

An M3C prototype with three full-bridge cells per branch is built up to validate the proposed control strategy. The circuit configuration and the experiment platform are shown in Fig. 4(a) and (b). The M3C prototype consists of a central controller and 27 full-bridge cells. The central controller includes a 32-bit digital signal processor TMS320F28377 and a field-programmable gate array chip. Each cell has a complex-programmable-logic-device-based cell controller. A central controller and cell controllers are connected in an optical-fiber-based ring network. In Fig. 4(a), S_3, S_5, and S_7 are mechanical breakers to disconnect branches 3, 5, and 7.

In Table II, the first and second columns summarize the M3C parameters and experiment conditions. For the specified *RL* Load in Table II, the φ_2 is 7.2°. In this case, the solution of the optimization problem in (7) after the loss of branch 3 is presented in the third column in Table II. Fig. 5(a) and (b) presents the experiment verification of the transition from the full M3C to the eight-branch topology and the transition from the full M3C to the Hexverter, respectively. The used capacitor-voltage balancing method is in [14] and [16].

In Fig. 5(a), before moment t_1, breaker S_3 is closed and the converter is operated as a normal M3C [breakers S_5 and S_7 remain closed in the whole process in Fig. 5(a)]. At moment t_1, breaker S_3 is still closed, but the branch current references are changed to the branch current configuration determined by the [k_{ij}] in Table II. It can be seen that the branch current i_{b3} becomes

close to zero from t_1. This helps to achieve a soft branch remove later. At moment t_2, the breaker S_3 is open. As can be seen, the branch current i_{b3} becomes zero immediately and the relative capacitor-voltage fluctuation disappears (see u_{c31}, where u_{c31} is the capacitor-voltage of the first cell in branch 3). Fig. 5(a) validates a smooth transition from a full M3C to the eight-branch topology and the stable operation of the reduced topology after the branch loss. In the whole process, there is no voltage and current spike. Besides, grid currents i_u, i_v, and i_w are in phase with grid voltages v_{Gu}, v_{Gv}, and v_{Gw}; therefore, unity power factor is ensured at the grid side.

For comparison, the results of the transition from the M3C to the Hexverter after the branch failure are shown in Fig. 5(b). Similar with the results of the transition from the M3C to the eight-branch topology, there are three stages in Fig. 5(b): before moment t_1, breakers S_3, S_5, and S_7 are closed, and the converter is operated as a normal M3C. At moment t_1, breakers S_3, S_5, and S_7 are still closed, but the branch current references are changed to the Hexverter branch current configuration, so i_{b3}, i_{b5}, and i_{b7} become close to zero. At moment t_2, breakers S_3, S_5, and S_7 are opened and branches 3, 5, and 7 are removed at the same time. The experiment comparison between the eight-branch topology and the Hexverter proves the significant advantage of the proposed method. As can be seen from Fig. 5(a) and (b), compared to the method of operating M3C as a Hexverter after a branch lost, the proposed strategy lowers the branch current peak-to-peak value by 16.49% (from 47.9 to 40 A), reduces the floating capacitor-voltage peak-to-peak value by 39.68% (from 63 to 38 V), and limits the peak-to-peak value of the injected CMV by 56.6% (from 530 to 230 V).

V. Conclusion

In this letter, the operation of the M3C as an eight-branch topology in the case of a branch loss is proposed and verified. A general optimization-based strategy is developed to provide an optimized branch current configuration after the branch failure. Compared to the method of operating the M3C as a Hexverter after a branch loss, the proposed strategy can lower the maximum branch current magnitude and improve the capacitor-voltage fluctuation; therefore, a smaller system power capability loss after the branch fault is achievable. Moreover, the CMV injection required by the Hexverter is completely avoided when unity power factor is required at the grid side. The proposed method can also be easily extended to two or more branch lost conditions, and the conception of the method is applicable for all the modular multilevel cascaded topologies.

References

[1] H. Akagi, "Classification, terminology, and application of the modular multilevel cascade converter (MMCC)," *IEEE Trans. Power Electron.*, vol. 26, no. 11. pp. 3119–3130, Nov. 2011.

[2] F. Kammerer, D. Braeckle, M. Gommeringer, M. Schnarrenberger, and M. Braun, "Operating performance of the modular multilevel matrix converter in drive applications," in *Proc. PCIM Europe 2015, Int. Exhib. Conf. Power Electron., Intell. Motion, Renew. Energy Energy Manage.*, 2015, pp. 1–8.

[3] K. Ilves, L. Bessegato, and S. Norrga, "Comparison of cascaded multilevel converter topologies for AC/AC conversion," in *Proc. Int. Power Electron. Conf.*, 2014, pp. 1087–1094.

[4] Y. Okazaki *et al.*, "Experimental comparisons between modular multilevel DSCC inverters and TSBC converters for medium-voltage motor drives," *IEEE Trans. Power Electron.*, vol. 32, no. 3, pp. 1805–1817, Mar. 2017.

[5] S. Liu, X. Wang, Y. Meng, P. Sun, H. Luo, and B. Wang, "A decoupled control strategy of modular multilevel matrix converter for fractional frequency transmission system," *IEEE Trans. Power Del.*, vol. 32, no. 4, pp. 2111–2121, Aug. 2017.

[6] K. Li, Z. Zhao, L. Yuan, S. Lu, and Y. Jiang, "Fault detection and tolerant control of open-circuit failure in MMC with full-bridge sub-modules," in *Proc. IEEE Energy Convers. Congr. Expo.*, 2016, pp. 1–6.

[7] J. Kucka, D. Karwatzki, and A. Mertens, "Optimised operating range of modular multilevel converters for AC/AC conversion with failed modules," in *Proc. 17th Eur. Conf. Power Electron. Appl.*, 2015, pp. 1–10.

[8] D. Karwatzki, M. von Hofen, L. Baruschka, and A. Mertens, "Operation of modular multilevel matrix converters with failed branches," in *Proc. 40th Annu. Conf. IEEE Ind. Electron. Soc.*, 2014, pp. 1650–1656.

[9] L. Baruschka and A. Mertens, "A new 3-phase AC/AC modular multilevel converter with six branches in hexagonal configuration," in *Proc. IEEE Energy Convers. Congr. Expo.*, 2011, pp. 4005–4012.

[10] L. Baruschka and A. Mertens, "A new three-phase AC/AC modular multilevel converter with six branches in hexagonal configuration," *IEEE Trans. Ind. Appl.*, vol. 49, no. 3, pp. 1400–1410, May/Jun. 2013.

[11] W. Kawamura, M. Hagiwara, and H. Akagi, "Control and experiment of a modular multilevel cascade converter based on triple-star bridge cells (MMCC-TSBC)," *IEEE Trans. Ind. Appl.*, vol. 50, no. 5, pp. 3536–3548, Sep./Oct. 2014.

[12] W. Kawamura, M. Hagiwara, and H. Akagi, "Control and experiment of a 380-V, 15-kW motor drive using modular multilevel cascade converter based on triple-star bridge cells (MMCC-TSBC)," in *Proc. Int. Power Electron. Conf.*, 2014, pp. 3742–3749.

[13] F. Kammerer, M. Gommeringer, J. Kolb, and M. Braun, "Energy balancing of the Modular Multilevel Matrix Converter based on a new transformed arm power analysis," in *Proc. 16th Eur. Conf. Power Electron. Appl.*, 2014, pp. 1–10.

[14] B. Fan, K. Wang, Y. Li, Z. Zheng, and L. Xu, "A branch energy control method based on optimized neutral-point voltage injection for a hexagonal modular multilevel direct converter (Hexverter)," in *Proc. 18th Int. Conf. Elect. Mach. Syst.*, 2015, pp. 1889–1893.

[15] D. Karwatzki, L. Baruschka, M. von Hofen, and A. Mertens, "Optimised operation mode for the Hexverter topology based on adjacent compensating power," in *Proc. IEEE Energy Convers. Congr. Expo.*, 2014, pp. 5399–5406.

[16] B. Fan, K. Wang, P. Wheeler, C. Gu, and Y. Li, "An optimal full frequency control strategy for the modular multilevel matrix converter based on predictive control," *IEEE Trans. Power Electron.*, vol. PP, no. 99. p. 1, 2017.